Nat Hazards (2013) 65:331–357
DOI 10.1007/s11069-012-0364-5

ORIGINAL PAPER

Real-time prediction of a severe cyclone 'Jal' over Bay of Bengal using a high-resolution mesoscale model WRF (ARW)

C. V. Srinivas · V. Yesubabu · K. B. R. R. Hariprasad · S. S. V. Ramakrishna · B. Venkatraman

Received: 29 March 2011 / Accepted: 17 August 2012 / Published online: 18 September 2012

Abstract Real-time predictions for the JAL severe cyclone formed in November 2010 over Bay of Bengal using a high-resolution Weather Research and Forecasting (WRF ARW) mesoscale model are presented. The predictions are evaluated with different initial conditions and assimilation of observations. The model is configured with two-way interactive nested domains and with fine resolution of 9 km for the region covering the Bay of Bengal. Simulations are performed with NCEP GFS 0.5° analysis and forecasts for initial/boundary conditions. To examine the impact of initial conditions on the forecasts, eleven real-time numerical experiments are conducted with model integration starting at 00, 06, 12, 18 UTC 4 Nov, 5 Nov and 00, 06, 12 UTC 6 Nov and all ending at 00 UTC 8 Nov. Results indicated that experiments starting prior to 18 UTC 04 Nov produced faster moving cyclones with higher intensity relative to the IMD estimates. The experiments with initial time at 18 UTC 04 Nov, 00 UTC 05 Nov and with integration length of 78 h and 72 h produced best prediction comparable with IMD estimates of the cyclone track and intensity parameters. To study the impact of observational assimilation on the model predictions FDDA, grid nudging is performed separately using (1) land-based automated weather stations (FDDAAWS), (2) MODIS temperature and humidity profiles (FDDAMODIS), and (3) ASCAT and OCEANSAT wind vectors (FDDAASCAT). These experiments reduced the pre-deepening period of the storm by 12 h and produced an early intensification. While the assimilation of AWS data has shown meagre impact on intensity, the assimilation of scatterometer winds produced an intermittent drop in intensity in the peak stage. The experiments FDDAMODIS and FDDAQSCAT produced minimum error in track and intensity estimates for a 90-h prediction of the storm.

C. V. Srinivas (✉) · K. B. R. R. Hariprasad · B. Venkatraman
Radiological Safety Division and Environment Group, Indira Gandhi Centre for Atomic Research, Kalpakkam 603102, India
e-mail: venkatasrinivasc@yahoo.com; cvsri@igcar.gov.in

V. Yesubabu
Computational Atmospheric Sciences Group, Centre for Development of Advanced Computing, Pune, India

S. S. V. Ramakrishna
Department of Meteorology and Oceanography, Andhra University, Visakhapatam 530003, India

Keywords Tropical cyclone · ARW · Real-time prediction · Data assimilation

1 Introduction

Tropical cyclones (TC) are one of the most violent weather manifestations that cause devastation along the coastal regions. The tropical storms form and develop over warm tropical oceans under favourable environmental conditions (Gray 1968). The Bay of Bengal (BOB) in the Indian Ocean is a potentially energetic region for the development of TCs and contributes about 7 % of the global annual tropical storms. The TCs in the Indian Ocean generally form during the pre-monsoon season in May and the post-monsoon season in October–November. The disaster from TCs is due to the extreme winds, torrential rains and occasional storm surge at the location of landfall along the coastal regions, which necessitates forecast-based lead time warnings to mitigate the disaster. Observational and modelling techniques are currently applied worldwide to provide advance information on the intensity and movement of these violent storms. The history of the past cyclonic storms indicates that the movement of the cyclones in the BOB is highly variable (Raghavan and Sen Sarma 2000), which makes their prediction a challenging problem. Numerical models of varied complexity have been developed and applied since 1960s to explain the physical and dynamical mechanisms of tropical cyclone development and movement. The present state of art is the application of non-hydrostatic nested-grid mesoscale models and the use of data assimilation methods to precisely simulate the various physical and dynamical processes of the storm environment and its evolution.

Tropical cyclone forecasts are being issued operationally by weather agencies of various nations (Iwasaki et al. 1987; Mathur 1991; Puri et al. 1992; Chen et al. 1995; Kurihara et al. 1993). In India, the India Meteorological Department (IMD) issues forecasts of the tropical cyclones over North Indian Ocean (NIO) using limited area models and with the assimilation of synthetic observations (Prasad and Rama Rao 2003). With the advent of high-performance computing high-resolution non-hydrostatic mesoscale atmospheric models such as MM5, WRF is being used for research and operational forecasting of several mesoscale atmospheric phenomena. Several studies are reported on the simulation/prediction of tropical cyclones over the NIO (Mohanty et al. 2004; Bhaskar Rao and Hari Prasad 2006, 2007; Srinivas et al. 2007; Bhaskar Rao et al. 2009a, b; Pattnayak and Rama Rao 2009; Deshpande et al. 2010; Srinivas et al. 2010a; among others). Tropical cyclone forecasting by numerical weather prediction models involves large errors in initial location of the storm, which arise due to poor availability of observational data in the sea areas where these storms develop (Prasad and Rama Rao 2003). Presently, models are used with the global analysis/forecasts as initial boundary conditions with integration times of 3–4 days to have lead time predictions. The accuracy of these forecasts depends on the initial data, which defines the state of the atmosphere describing the cyclone vortex. Because of the poor coverage of observations over the ocean region and the resultant poor representation of location and characteristics of the initial low pressure (i.e., cyclone vortex) in the coarse grid global analysis, it is often difficult to detect the incipient stage of a storm and to predict its further development using the numerical models. The poor representational errors in the global analysis result in the underestimation of time of origination, strength and position of the cyclone vortex, making it difficult to forecast tropical cyclones precisely. In other words, the skill of model forecasts depends to some extent on the observational analysis and its time which is used as initial condition. A comparative study with

MM5 and WRF mesoscale models was attempted by Pattnayak and Mohanty (2008) for the prediction of SIDR cyclone with initial conditions from 13 to 14 November 2007, which reported that WRF performs better than the MM5 model in the simulation of intensity and movement in close agreement with IMD estimates. Bhaskar Rao et al. (2009b) made a real-time prediction of SIDR cyclone using MM5 and WRF models using different initial conditions starting from 00 UTC of 11 through 14 November 2007 and inferred that WRF performs better than MM5 in terms of producing higher intensity. Davis et al. (2008) studied the performance of the WRF ARW model with real-time forecasts of five land-falling Atlantic hurricanes during 2005. They found that the performance of ARW is generally competitive with, and occasionally superior to, other operational forecasts for storm position and intensity.

The major improvements in NWP as also for cyclone forecasting during the last 15 years are attributed to the development of various sources of observations and the data assimilation methods to effectively use them. Data assimilation helps to precisely define the initial conditions to numerical weather prediction (NWP) models by combining all available past as well as current observations to best define the initial state of the atmosphere (Kalnay 2003). A review of different data assimilation methods such as successive correction, optimum interpolation and variational methods (3-D VAR, 4-DVAR) and their application in NWP models was given by Navon (2009). A general problem in the numerical modelling of tropical cyclones is the deficiency of conventional observations over the oceanic regions where cyclones form and develop. With the advent of satellite remote sensing, the observational gap over the oceans has been greatly reduced. Satellite observations provide a very useful data for understanding and simulation of tropical cyclones. An overview on the impact of assimilation of satellite data for tropical cyclone simulations, the current problems associated with satellite data assimilation, recent developments and prospects has been given by Pu (2009). Satellite observations are highly useful because of their high spatial coverage, repetition and resolution. Satellite scatterometer-based wind observations and the temperature/humidity profiles are a potential source of data over oceanic regions since it provides crucial information in the form of wind speed and direction for correcting the initial location of the storm. The OCEANSAT-2 scatterometer provides surface winds over the Indian Ocean region at a 50-km resolution and accuracy of 1 m/s. The ocean surface wind observations from OCEANSAT-2 find potential application in defining the vortex of a developing storm in numerical models. The temperature and humidity profiles from TOVS and MODIS have been found to be useful to define the thermodynamical structure of the developing storms. The conventional observations over the land region can be used to enhance the input fields for precise initial conditions in models. In addition to the large amount of satellite information, assimilation of dropwindsonde data deployed from surveillance aircrafts is highly important in numerical forecast of tropical cyclones as reported in several studies (Wu et al. 2007; Park et al. 2008; Kim et al. 2010 among others).

Several studies reported the advantages of using satellite observations in defining the initial conditions of brewing tropical storms and their simulation (Leslie et al. 1998; Marshall et al. 2000; Soden et al. 2001; Zhihua et al. 2005; Langland et al. 2009; etc.). Leslie et al. (1998) have shown that the track of a hurricane could be better simulated with the assimilation of high temporal and spatial resolution GOES satellite-derived wind vectors using FDDA nudging. Marshall et al. (2000) using nudging of scatterometer winds had shown that the initial position error of cyclone was substantially reduced. In a modelling study of Typhoon Dujan using the NCAR MM5, Zhihua et al. (2005) reported that assimilation of QSCAT wind data produced significant impacts on the model storm

structure for horizontal and vertical winds, sea level pressure, temperature and improvement in the intensity and track prediction. Zhang et al. (2007) have studied the individual impacts of a number of satellite data on winds, temperature profiles on the initialization and forecasting of the rapid weakening of Hurricane Lili-2002 using the PSU/NCAR model MM5. Langland et al., (2009) conducted a series of data assimilation and forecasting experiments to study the impact of GOES rapid-scan wind observations on the simulation of track of hurricane Katrina. In recent times, several studies on simulation of cyclones and monsoon depressions are reported over the North Indian Ocean region (e.g., Roy Bhowmik 2003; Mukhopadhyay et al. 2004; Sandeep et al. 2006; Vinodkumar et al. 2007; among several others). Singh et al. (2008) have reported that the assimilation of QSCAT and SSM/I winds improves the position of the initial vortex, its strength leading to significant improvements in the intensity and track predictions for Orissa super cyclone.

It is well known that tropical cyclone characteristics drastically change at different stages in the life cycle. Often it is difficult to predict the intensity and motion of tropical cyclones especially from deepening period to mature stage and from mature stage to dissipation stage. Hence, it is necessary to evaluate models by simulating the entire life cycle with different initial conditions. In this study, an attempt is made to study the near real-time prediction of tropical cyclone JAL that formed in November 2010 over Bay of Bengal using the NCAR WRF mesoscale model with an objective to study the model predictions of the intensification and movement of the tropical cyclone with eleven initial conditions starting at 00, 06, 12, 18 UTC 4 Nov, 00, 06, 12, 18 UTC 5 Nov and 00, 06, 12 UTC Nov and the impact of individual FDDA analysis nudging of OCEANSAT-2 wind observations, MODIS profiles and conventional land-based observations for the initial time at 06 UTC 4 Nov. Separate assimilation experiments are conducted with individual data sets to study the contribution of different data to the predictions.

2 Description of the severe cyclone 'Jal'

JAL is a severe cyclonic storm formed in the Bay of Bengal and had a life cycle during 4–8 November 2010, with a minimum central sea level pressure (CSLP) of 988 hPa and maximum sustained wind speed (MSW) of 60 knots ($\sim$30 m/s; IMD 2011). The system originated as a well-marked low pressure at 12 UTC 2 Nov, over south Bay of Bengal. It became a depression over southeast BOB at 00 UTC 4 Nov and lay centred at Lat. 8.5 N and Long. 91.0 E. It moved in a west-northwestward direction and concentrated into a deep depression over southeast BOB at 00 UTC 5 Nov and lay centred at Lat. 9.00 N and Long. 88.50 E. Thereafter, it moved in a westward direction and intensified into a cyclonic storm (JAL) at 12 UTC 5 Nov and lay centred at Lat. 9.5 N and Long. 87.0 E. It further moved west northwestwards and intensified into a severe cyclonic storm (SCS) over southeast Bay of Bengal at 00 UTC 6 Nov (Fig. 1). The system then moved first westwards and then moved very slowly northwestwards, weakened into a cyclonic storm on 06 UTC 7 Nov near Lat. 12.5 N and Long. 82.5° E. The system continued to move northwestwards and made landfall north of Chennai coast at Lat. 13.30 N and Long. 80.20 E around 16 UTC 7 Nov. Thereafter, moving in a west-northwestward direction, it got weakened into a depression over Rayalaseema of south Andhra Pradesh. The system moved very slowly during its post-intensification stage and remained stationary over the ocean for a day. Due to this cyclone, about 50 casualties were reported besides heavy loss of crop damage in south coastal Andhra Pradesh.

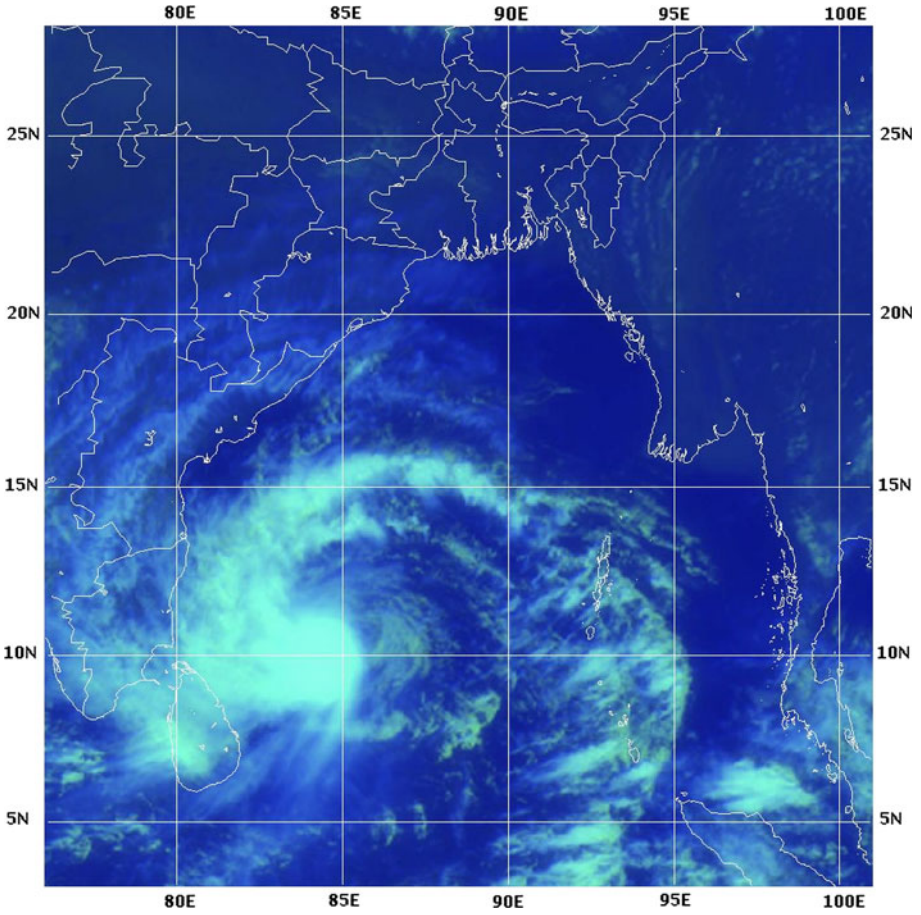

Fig. 1 INSAT VHRR picture of cyclone 'Jal' at 06 UTC of 6 Nov 2010

3 Brief description of the ARW model and its configuration

The Advanced Research Weather Research and Forecast (ARW) v3.2 mesoscale model developed by the National Center for Atmospheric Research (NCAR) (Skamarock et al. 2008) is used in this study. The model consists of fully compressible non-hydrostatic equations, and the prognostic variables include the three-dimensional wind, perturbation quantities of pressure, potential temperature, geo-potential, surface pressure, turbulent kinetic energy and scalars (water vapour mixing ratio, cloud water etc.). The model has a terrain following vertical coordinate and Arakawa C-grid staggering in the horizontal. A third-order Runge–Kutta time integration is used in the model. The model has several options for spatial discretization, diffusion, nesting and lateral boundary conditions besides number of physics. For the present study the model is configured with two interactive nested domains. The outer domain covers a larger region with 27-km resolution and 192×192 grids. The inner domain has 9-km resolution with 289×289 grids covering the Bay of Bengal and its environments (Fig. 2). A total of 42 vertical levels are used. The physics schemes used in the present study are Yonsei University (Hong et al. 2006)

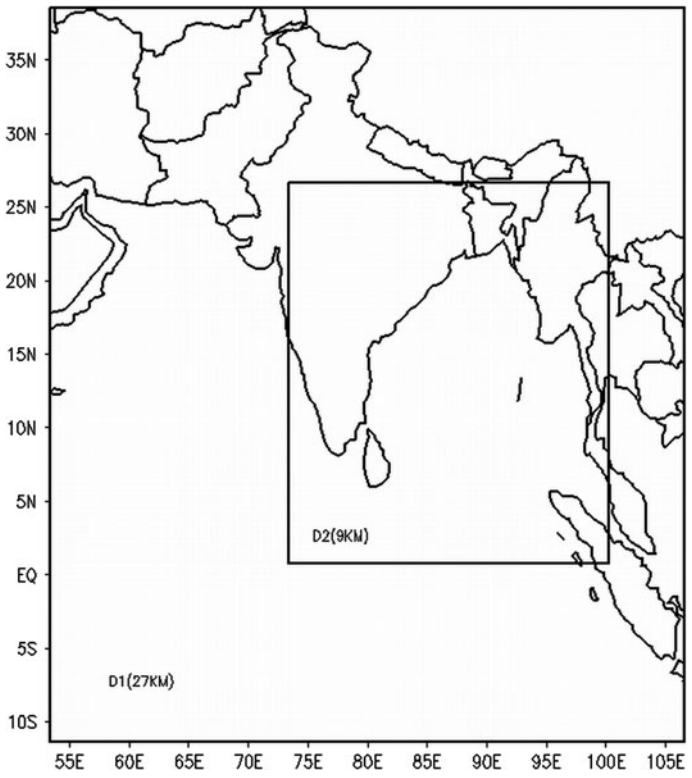

Fig. 2 Domains used in the WRF (ARW) model

non-local diffusion scheme for PBL processes, Kain–Fritsch (KF-Eta) (Kain and Fritsch 1993; Kain 2004) for cumulus convection, Purde Lin scheme (Lin et al. 1983) for explicit moisture processes, five-layer soil thermal diffusion model for surface processes, Rapid Radiation Transfer Model (RRTM) for long-wave radiation (Mlawer et al. 1997) and Dudhia (1989) scheme for shortwave radiation.

4 Numerical experiments

Two different sets of numerical simulations are carried out with WRF model. In the first set, eleven real-time numerical prediction experiments are conducted with static initialization of WRF using the National Centers for Environmental Prediction (NCEP) Global Forecast System (GFS) analysis and 6 hourly forecasts available at a $0.5° \times 0.5°$ latitude–longitude grid. The time-varying SST data over all the domains are also defined from the GFS data. The GFS follows 4 analysis cycles (00, 06, 12, 18 UTC), and the forecasts corresponding to each analysis cycle are available up to 7 days at 3-h intervals. In the first set of experiments, model simulations are made starting at 00, 06, 12, 18 UTC 4 Nov, 00, 06, 12, 18 UTC 5 Nov, 00, 06, 12 UTC 6 Nov 2010, with corresponding GFS analysis cycle data sets, and the model is integrated up to 00 UTC 8 Nov in each case. The intensity

Table 1 Details of domains and physics used in the model

Dynamics	Primitive equation, non-hydrostatic	
Vertical resolution	42 vertical levels	
Horizontal resolution	27 km	9 km
Domains of integration	72.643°E–94.504°E 3.5315° N–24.377° N (192 × 192 grids)	76.20°E–88.84°E 5.595° N–18.81°N (289 × 289 grids)
Radiation	Dudhia scheme for short-wave radiation Rapid radiation transfer model (RRTM) for long-wave radiation	
Explicit moisture	Lin scheme	
Surface processes	NOAH land surface model	
Planetary boundary layer	Yonsei University (YSU)	
Cumulus convection	Kain–Fritsch	
Sea surface temperature	Real SST	
Initial conditions		
real-time predictions	00, 06, 12, 18 UTC 4 Nov, 00, 06, 12 UTC 5 Nov	
Assimilation runs	06 UTC 4 Nov for Control run (CTL) FDDA experiments : 18 UTC 3 Nov to 06 UTC 4 Nov nudging, actual forecast begins from 06 UTC 04 Nov	

and track position estimates of the storm are taken from the daily reports of the India Meteorological Department (IMD) for comparison of model results (Table 1).

In the second set of experiments, four-dimensional data assimilation (FDDA) analysis nudging is performed separately with four different sources of data as described below. FDDA is a continuous data assimilation technique in which the model state is relaxed towards the observed state by augmenting some of the prognostic equations with forcing terms based on the difference between the observed state and the model state. In the control experiment, a static initialization of WRF is performed with initial condition at 06 UTC 4 Nov using GFS analysis. The model is integrated for a 90-h period up to 00 UTC 8 Nov with time-varying boundary conditions taken from GFS forecasts corresponding to the same analysis cycle. In the second experiment, the land-based AWS observations from ISRO and IMD are used in assimilation with a nudging interval of 3 h. In the third experiment, the OCEANSAT-2 and ASCAT scatterometer wind observations are used in FDDA assimilation with 12-h nudging interval. In the fourth experiment, the MODIS vertical profiles of temperature and humidity are used in assimilation with nudging interval of 12 h. The nudging interval is chosen as per the availability of observations in each case. The details of kinds of observations/variables assimilated in each experiment are given in Table 2. The distribution of various observations used in the assimilation experiments for a typical time at 18 UTC 03 Nov is given in Fig. 3.

OCEANSAT-2 microwave scatterometer is launched by Indian Space Research Organization (ISRO) and has been operational since 23 September 2009 (http://218.248.0.134:8080/OCMWebSCAT/html/controller.jsp). It has a swath width of 1,800 km, measures wind speed and direction at 10 m above ocean surface with a resolution of 50 km, retrieval accuracy of 1 m/s for wind speed (range, 4–24 m/s) and 20° for wind direction.

Table 2 Details of observations used in various numerical experiments

Experiment	First guess/ analysis	Type of observations	Variables in assimilation
Real-time runs	GFS	-nil-	-nil-
Control run	GFS	-nil-	-nil-
FDDASCAT	GFS	ASCAT, OCEANSAT-2	Ocean surface vector winds
FDDAMODIS	GFS	MODIS profiles	Temperature, humidity profiles
FDDAAWS	GFS	IMD AWS, ISRO AWS	Land-based surface data on vector winds, air temperature and humidity

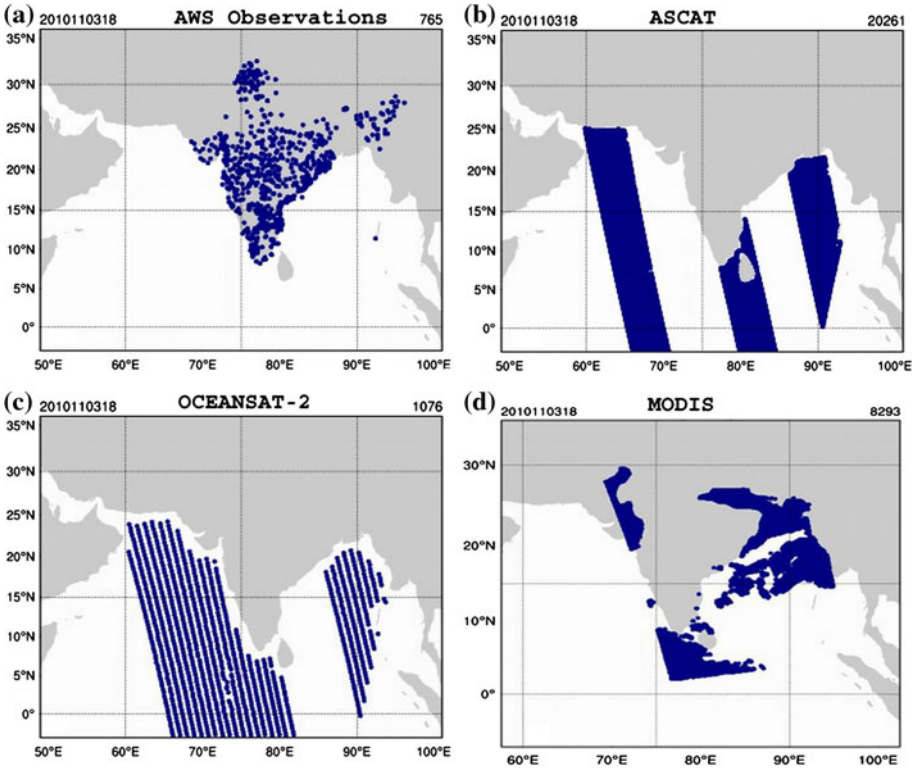

Fig. 3 Distribution of various observations used for assimilation **a** AWS data, **b** ASCAT winds, **c** OCEANSAT winds and **d** MODIS temperature, humidity profiles at 18 UTC 03 Nov

The Advanced Scatterometer (ASCAT) is part of the payloads of the Meteorological Operational (Metop) polar satellites launched by the European Space Agency (ESA) and operated by the European Organization for the Exploitation of Meteorological Satellites (EUMETSAT), and constitutes the space segment of EUMETSAT's Polar System (EPS). ASCAT is a real aperture radar operating at 5.255 GHz (C-band) with system geometry

based on the use of fan-beam antennas. The system covers two 550-km swaths separated by about 700 km (OSISAF 2010; Bi et al. 2010; Takahashi 2010). Both the morning and the evening passes of satellite wind data are used in assimilation. A network of Automated Weather Stations (AWS) has been set up by ISRO and has been used for the prediction of short-range weather and atmospheric dispersion (Kusuma Rao 2008; Srinivas et al. 2010b). Over the land region about 720 AWS observations from IMD and ISRO are used in assimilation (Fig. 3a).

In this work, FDDA analysis nudging is used, in which the model solution is nudged towards time- and space-interpolated analyses using a point-by-point relaxation term (Stauffer and Seaman 1990, 1994; Stauffer et al. 1991). In the analysis, nudging Newtonian relaxation terms are added to the prognostic equations for wind (u, v), temperature (t), water vapour (q) using the equation,

$$\frac{\partial \alpha}{\partial t} = F(\alpha, X, t) + G_\alpha W(X, t)\varepsilon(x)p * (\alpha_o - \alpha), \tag{1}$$

where 'α' is a prognostic variable (u, v, t, q), F denotes the normal tendency terms due to physics, advection, X are the independent spatial variables, and 't' is time. The second term on the right side of (1) represents the analysis nudging term for 'α'. The observations are interpolated using the standard Cressman objective analysis procedure with the first guess fields to prepare revised analysis files for use in FDDA analysis nudging. The objective interpolation of observations on the first guess fields is applied at the surface and at the mandatory and supplementary analysis pressure levels aloft (when MODIS profiles are used). In the experiments where MODIS profiles are used, the objective analysis considers the upper air observations. In the analysis nudging experiment surface and 3D grid nudging is performed for winds, temperature and humidity over the model domains. The nudging coefficient for wind speed, direction, temperature and mixing ratio is specified as 3.0e−4, which is the default value of the code and corresponds to a time scale of about 1 h. The actual model forecast begins from 06 UTC 04 Nov for a 90-h period ending at 00 UTC 08 Nov. The assimilation experiments are named as FDDAAWS (with AWS data), FDDA-SCAT (with satellite scatterometer winds), FDDAMODIS (with MODIS temperature, humidity profiles). The estimates from IMD for intensity, track parameters and rainfall are used for model comparisons.

5 Results

Results from real-time prediction experiments for the JAL cyclone are presented first, followed by the assimilation experiments. The real-time predictions are made during the life cycle of JAL over Bay of Bengal. As already discussed in previous section, a total of eleven predictions are attempted corresponding to the initial conditions at 00 UTC, 06 UTC, 12 UTC, 18 UTC 4 Nov, 00 UTC, 06 UTC, 12 UTC, 18 UTC 5 Nov, 00 UTC, 06 UTC, 12 UTC, 18 UTC 6 Nov, and model integrations ending at 00 UTC 08 Nov. The results for this set of experiments were referenced to time as hh UTC DD Nov, where hh UTC is the UTC time in hours and DD is the day. The intensity of simulated cyclone from different experiments is evaluated in terms of the minimum central sea level pressure (CSP), vorticity, maximum sustained winds (MSW) and radius of maximum wind (RMW). The IMD estimates for MSW were used for model comparison and validation. The time evolution of each of these four parameters for each of the experiments is discussed below.

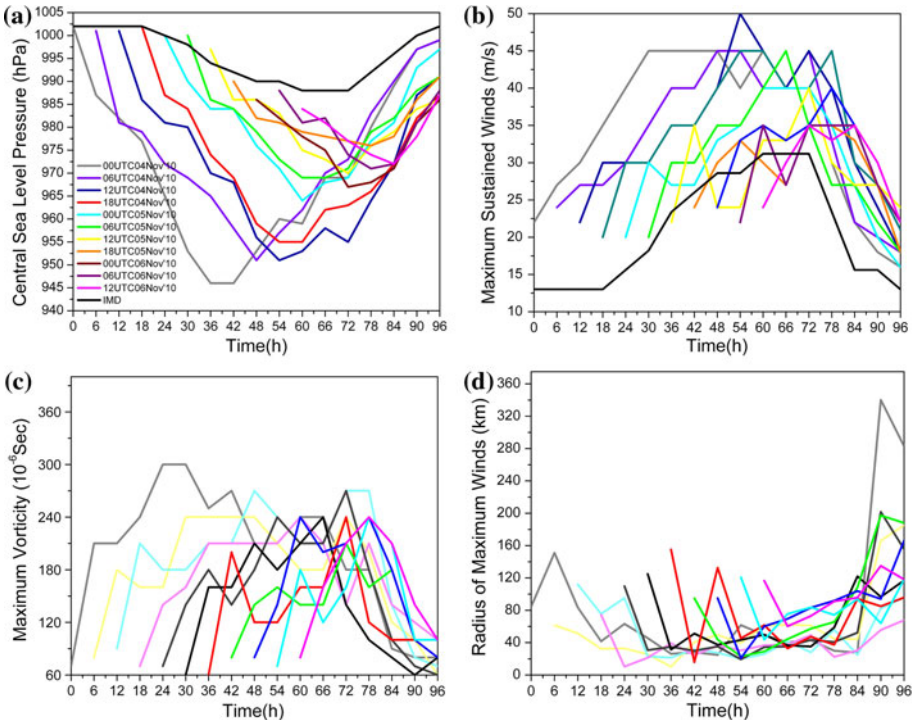

Fig. 4 Time evolution of **a** MSLP, **b** MSW, **c** Vorticity and **d** radius of maximum winds from different real-time prediction experiments

5.1 Real-time prediction experiments

5.1.1 Intensity of predicted storm

The time series of CSLP for the ten prediction experiments is presented in Fig. 4a. The time series from different experiments indicates that the experiment 00 UTC 04 Nov produces the lowest CSLP of 948 hPa after 39 h of integration and the experiment 18 UTC 05 Nov produces the highest CSLP of 975 hPa with all the successive experiments in the series having intermediate CSLP values. Accordingly, the pre-deepening period was noted to vary from 20 (for 00 UTC 04 Nov) to 9 h (for 18 UTC 05 Nov) for the above series of experiments. The experiments with initial conditions subsequent to 00 UTC 04 Nov have successively higher CSLP and lower pressure drop, thus indicating to have lower intensification. The peak intensification in different prediction experiments seems to occur successively at 6 h later relative to the experiment 00 UTC 04 Nov. As per the description of the storm available from IMD report (IMD 2011), the storm had attained peak intensity of severe cyclone between 00 UTC 06 Nov and 00 UTC 07 Nov and gradually weakened thereafter. Of all the eleven cases in the series, the experiments 00 UTC 05 Nov and 06 UTC 05 Nov are noted to give better comparison of the time variation in pressure (fall and rise in CSLP) to IMD observations of the storm. The time variation of MSW from different real-time prediction experiments along with the IMD estimates (IMD 2011) is presented in Fig. 4b. The MSW from IMD estimates indicates an increase in wind speed from 13 (at 18

UTC 4 Nov) to 31 m/s (at 12 UTC 06 Nov), which remained steady till 00 UTC 07 Nov. A steep increase in MSW from 17 to 30 m/s from 12 UTC 05 Nov to 12 UTC 06 Nov is noted in the IMD estimates. The maximum intensity of 30 m/s was maintained till 00 UTC 07 Nov and the intensity decreased exponentially thereafter. The time series of maximum winds from various experiments indicates that all of them overestimate the intensity. The experiments 00 UTC 04 Nov and 06 UTC 04 Nov both show increase in winds from 22 m/s attaining a highest intensity of 45 m/s at 00 UTC 06 Nov. However, both these experiments show an early intensification and an early weakening than the actual cyclone. Both these experiments indicate higher maximum winds by about 5–15 m/s throughout the intensification phase than the corresponding values from IMD estimates. The experiment starting at 00 UTC 04 Nov indicates a fall in maximum winds after 00 UTC 06 Nov, which after 12 UTC 06 Nov again increased to the peak intensity at 18 UTC 06 Nov. The experiment 12 UTC 04 Nov shows intensification slightly earlier to the actual storm (with two peaks of intensification), while 18 UTC 04 Nov, 00 UTC 05 Nov, 06 UTC 05 Nov provide similar growth and decay trends of intensification as in IMD observations, though the simulated winds are slightly more stronger than the IMD estimates. However, of these three experiments, the experiment starting at 18 UTC 04 Nov indicates relatively higher winds during the life cycle of the cyclone than the other two. The experiment 18 UTC 04 Nov produced a more realistic time evolution of MSW very closely following the IMD estimates. As per IMD estimates, the mature stage of the storm is between 12 UTC 06 Nov and 00 UTC 08 Nov, which is predicted by all the above three experiments (18 UTC 04 Nov, 00 UTC 05 Nov and 06 UTC 05 Nov). The experiments starting subsequent to 06 UTC 05 Nov all produced successively far lesser intensification compared to those starting earlier to 06 UTC 05 Nov with the experiment 12 UTC 06 Nov, producing the lowest intensity of all with predicted MSW of 35 m/s. From the above series of simulations, it is noted that experiments starting at different times during the life cycle of the cyclone have given different results. Experiments starting in the pre-deepening stage (low pressure) of the actual storm (i.e., prior to 00 UTC 05 Nov) produced an early intensification as well as early decay with an overall higher intensification in comparison with the observed characteristics. On the other hand, experiments starting in the mature stage/severe cyclone stage (i.e., after 12 UTC 06 Nov) have produced a late intensification of the storm with relatively less intensification. The errors in the early phase experiments may be attributable to the quality of initial conditions, model dynamics as well as the model physics. The errors in the late phase experiments may be because of less spin-up time for the model to evolve the development of cyclone. Strikingly, all the experiments starting in the deepening phase (18 UTC 04 Nov to 18 UTC 05 Nov) produced more realistic simulation of the life cycle in terms of representation of the growth and decay characteristics than the rest. These results strongly suggest that numerical models used in short-range predictions of cyclones need to have a minimum integration time of 2 days with initial conditions preferably defined at the pre-deepening/deepening phase to evolve a proper life cycle of the storm.

The time evolution of the maximum vorticity of the storm at 925 hPa from different real-time prediction experiments is given in Fig. 4c. Generally, the vorticity of the storm gradually grows during the intensification phase, attains a peak value during the stages of highest intensification and then gradually falls during the weakening phase of storm according to the wind circulation and the attained maximum winds of the storm. From the time series, it is noted that the highest vorticity is predicted at different times in different experiments as per the life cycle simulated in each experiment. The highest vorticity was attained at 18 UTC 05 Nov, 00 UTC 06 Nov, 12 UTC 06 Nov, 00 UTC 06 Nov, 15 UTC 06 Nov, 21 UTC 06 Nov and at 18 UTC 06 Nov, respectively, in the experiments starting at

00 UTC 04 Nov, 06 UTC 04 Nov, 12 UTC 05 Nov, 18 UTC 05 Nov, 00 UTC 05 Nov, 06 UTC 05 Nov and 12 UTC 05 Nov, respectively. The experiments starting at various times on 4 November showed the higher vorticity between 12 UTC 05 Nov and 12 UTC 06 Nov, whereas the rest of the experiments indicated higher vorticity between 12 UTC 06 Nov and 12 UTC 07 Nov. The highest attained vorticities in various real-time prediction experiments are $270 \times 10^{-5}\ s^{-1}$, $245 \times 10^{-5}\ s^{-1}$, $240 \times 10^{-5}\ s^{-1}$, $280 \times 10^{-5}\ s^{-1}$, $235 \times 10^{-5}\ s^{-1}$, $230 \times 10^{-5}\ s^{-1}$ and $210 \times 10^{-5}\ s^{-1}$ in the experiments 00 UTC 04 Nov, 06 UTC 04 Nov, 12 UTC 05 Nov, 18 UTC 05 Nov, 00 UTC 05 Nov, 06 UTC 05 Nov and 12 UTC 05 Nov, respectively. The experiments 18 UTC 04 Nov and 00 UTC 05 Nov are found to provide the trend of a gradually growing vorticity during the intensification phase and gradually decaying vorticity during the weakening phase of the storm and hence produced a more realistic time variation of vorticity associated with the cyclone.

The distance between the centre of tropical cyclone (core region) and its band of strongest winds, called radius of maximum winds (RMW), is an important measure of its intensity especially when the cyclone is about to strike the coast. The time evolution of RMW associated with the predicted storm from different experiments is plotted in Fig. 4d. All the experiments except the one starting at 12 UTC 05 Nov indicate a lower RMW in the developing and mature stages and a higher RMW during the decaying stage of the storm. It has been found that experiments starting at 18 UTC 04 Nov and 00 UTC 05 Nov followed by 12 UTC 04 Nov produced the lowest RMW of about 50–80 km during the peak intensification stage and also more realistic values of RMW during the weakening phase.

5.1.2 *Movement of the predicted storm*

The movement of the predicted cyclone from real-time simulations is analysed by comparing the track positions of the storm along with the corresponding positions from IMD

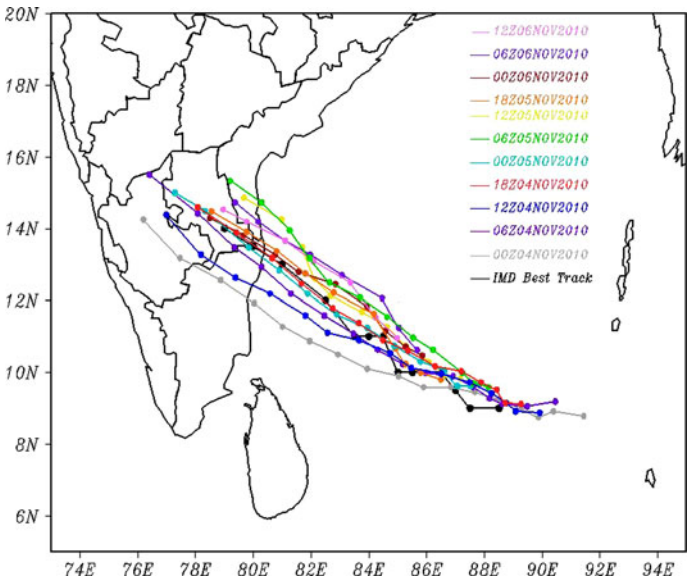

Fig. 5 Track positions of the simulated storm from different real-time prediction experiments

Table 3 Vector track errors in the real-time prediction experiments

Simulation	Vector track errors (in km)								
	Hours of simulation								
	00	12	24	36	48	60	72	84	96
00 UTC 04 Nov	106.81	30.16	27.75	20.72	54.19	183.69	278.63	241.60	313.04
06 UTC 04 Nov	75.72	116.91	67.59	63.76	104.78	179.49	275.96	239.28	
12 UTC 04 Nov	42.93	32.45	59.27	14.62	95.17	199.14	184.98	227.38	
18 UTC 04 Nov	73.08	117.92	77.37	76.98	57.07	106.33	116.81		
00 UTC 05 Nov	105.39	14.38	45.49	67.79	223.44	149.33	220.47		
06 UTC 05 Nov	96.09	81.33	122.86	125.41	143.13	193.44			
12 UTC 05 Nov	39.85	71.65	33.40	154.57	93.09	120.37			
18 UTC 05 Nov	22.95	39.16	72.22	113.54	102.99				
00 UTC 06 Nov	64.91	18.14	177.08	40.72	64.61				
06 UTC 06 Nov	101.37	128.55	152.92	133.14					
12 UTC 06 Nov	53.47	167.07	73.58	58.42					

best-track estimates. Figure 5 gives the track positions of the predicted storm from various experiments. As the initial conditions in the real-time simulations are at different analysis times, it is obvious that the location of the initial cyclone vortex would not be identical. A positional difference in the initial location of the storm depending on the rate of actual storm movement is expected at the start of each experiment. From the IMD estimated track positions, it is noted that the storm was originally located in the east Bay of Bengal, in Andaman sea at around 91° E, 8.5° N, and gradually moved in a west-northwestward direction in a duration of 24 h. The initial track positions from various experiments are convergent till the first 24 h of the storm. Interestingly, subsequent to 00 UTC 05 Nov, the vector tracks became divergent. The predicted cyclone tracks in the experiments with initial time prior to 00 UTC 05 Nov are to the south of the IMD estimated track and those from experiments with start time subsequent to 00 UTC 05 Nov are to the north of the predicted storm, with successive northward incremental drifts in the track positions. Further it is noted that the simulated storm in all experiments moved faster than the observed storm and indicates considerable errors along the track. The vector track errors gradually increased from initial time in various experiments. The largest errors are noted with 00 UTC 04 Nov, 12 UTC 04 Nov, 06 UTC 04 Nov, 06 UTC 05 Nov and 12 UTC 05 Nov, respectively (Table 3). The large track errors (150–313 km) after 48 h of simulation in the experiments 00 UTC 04 Nov, 12 UTC 04 Nov and 00 UTC 05 Nov are due to the faster forward movement of simulated cyclone than the actual cyclone. The fast movement of simulated storm may be due to the strong upper air boundary forcing which needs to be examined further. The experiments 00 UTC 05 Nov, 06 UTC 05 Nov and 12 UTC 05 Nov produced marginal errors for integrations up to 60 h. The track errors for these cases are due to the northward drift of the storm from the actual track. The experiments 18 UTC 04 Nov and 00 UTC 05 Nov indicated marginal errors right from the beginning of the simulations, the predicted tracks almost agree with the IMD estimated track, but slightly to the south of the actual track. As per the IMD estimates, the cyclone initially moved westwards, to the northwest, and remained stationary for a long time. It then moved slowly in a northwestward direction and crossed coast just north of Chennai as per the

Table 4 Mean errors in vector track position, maximum winds and central pressure from 11 real-time prediction experiments

Simulation	Mean prediction errors							
	Hours of simulation							
	12	24	36	48	60	72	84	96
Track (km)	74.34	82.69	79.06	104.27	161.68	215.37	236.08	313.04
Max. wind (m/s)	−13.3	−14.4	−10.0	−6.5	−6.3	−7.5	−13.8	−6.5
Central pressure (hPa)	14.0	19.0	19.5	20.2	19.0	18.5	18.0	11.0

observations. This trend in the movement of the simulated cyclone could be very closely predicted by the experiment 18 UTC 04 Nov with least track errors in the simulation. Thus, considering both the intensity and the movement, the simulation 18 UTC 04 Nov produced the best prediction followed by 00 UTC 05 Nov. These real-time prediction experiments indicate that it is highly important to choose a proper initial time for the near real-time forecasts of the probable landfall point of a tropical cyclone with numerical models. Experiments starting before 18 UTC 04 Nov have southward drift of model storm, while those starting after 18 UTC 04 Nov have northward drift of the model storm to the actual observed storm. The simulated tracks from real-time experiments indicate relatively faster storm in the experiments starting prior to 18 UTC 04 Nov. The mean track errors for 12-, 24-, 48-, 72-, 96-h predictions are found to vary as 74, 83, 104, 215 km, respectively. The mean wind errors are found to be −13.3, −14.4, −6.5, −7.5 and −6.5 ms^{-1} for 12-, 24-, 48-, 72-, 96-h predictions, respectively. The corresponding mean central pressure errors are 14, 19, 20.2, 18.5 and 11.0 hPa, respectively (Table 4). The initial track position errors are found to range from 107 to 96 km for the experiments prior to 06 UTC 05 Nov and from 22 to 53 km for the subsequent experiments. Given these large initial errors, the experiments starting prior to 06 UTC 05 Nov are associated with large track errors.

5.1.3 Rainfall of predicted storm

The predicted rainfall pattern from different real-time experiments during the landfall time is compared with TRMM rainfall pattern. Figure 6 gives the accumulated predicted rainfall for the 24-h period from 00 UTC 07 Nov to 00 UTC 08 Nov from eleven experiments along with the corresponding TRMM measured rainfall. The precipitation in tropical storms generally occurs around the wall cloud region of the cyclone due to organization of horizontal winds and clouds in spiral bands around a relatively calm wind central eye region characterized with subsiding vertical motion. The TRMM data for 00 UTC 08 Nov indicate concentration of highest precipitation ($\geq$200 mm) along the north Tamil Nadu coast and the adjoining land, ocean regions. The precipitation has reduced from the central region, and rainfall of 120 to 10 mm is spread in the entire southern peninsular India except parts of extreme south Tamil Nadu and south Kerala, which remained dry. A second spatial peak of rainfall is located along the north coastal Andhra Pradesh around Visakhapatnam due to north and northeastward extension of rain bands. All the experiments show this rainfall distribution, indicating maximum rainfall in the central eye wall region around the simulated storm location. In the experiments starting at 00 UTC 04 Nov and 06 UTC 04 Nov, the central rainband appears to have shifted about 250 km inland in the

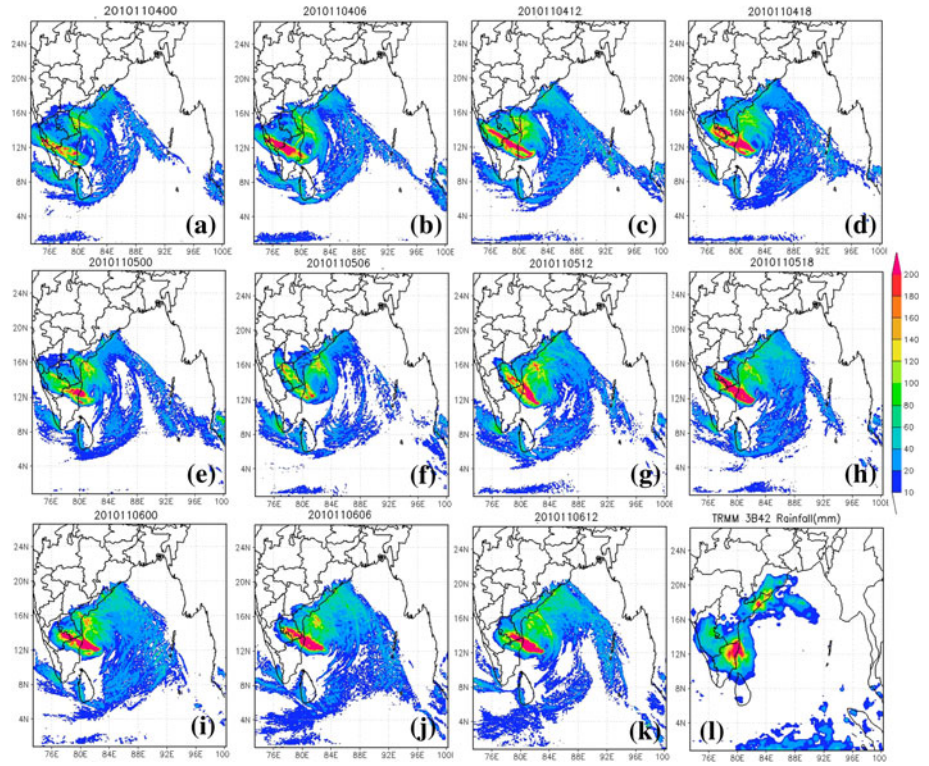

Fig. 6 Model simulated rainfall accumulated for the 24-h period ending at 00 UTC 08 Nov from **a** 00 UTC 04 Nov, **b** 06 UTC 04 Nov, **c** 12 UTC 04 Nov, **d** 18 UTC 04 Nov, **e** 00 UTC 05 Nov, **f** 06 UTC 05 Nov, **g** 12 UTC 05 Nov, **h** 18 UTC 05 Nov, **i** 00 UTC 06 Nov, **j** 00 UTC 06 Nov, **k** 06 UTC 06 Nov and **l** TRMM rainfall

northwest direction from the observed peak rainfall pattern, and the simulated rainfall in these two cases is under estimated by 50 mm. This indicates the model storm has moved faster than the actual one in the above experiments. In the experiments 12 UTC 04 Nov and 18 UTC 04 Nov, the location of the central rain band is accurately simulated but it is elongated in the northwest and southeast directions from the central maximum. The highest precipitation in these two experiments has spread to a larger region, and the rainfall is also confined to the northern Tamil Nadu and south Andhra Pradesh. In the experiment 00 UTC 05 Nov, the rainfall maximum could be simulated well but the rainfall distribution is localized and precipitation is under estimated. In the remaining experiments that started subsequent to 00 UTC 05 Nov, the zone of maximum rainfall is simulated to the north of Chennai and giving less aerial coverage to southern Tamil Nadu. Model rainfall comparison with TRMM data, however, needs to be made carefully as it has limitation in representing the low and moderate rainfall.

5.2 Assimilation experiments

In the second set of simulations, a control run and three FDDA grid nudging experiments are conducted. As per results obtained in the real-time predictions, the FDDA runs using

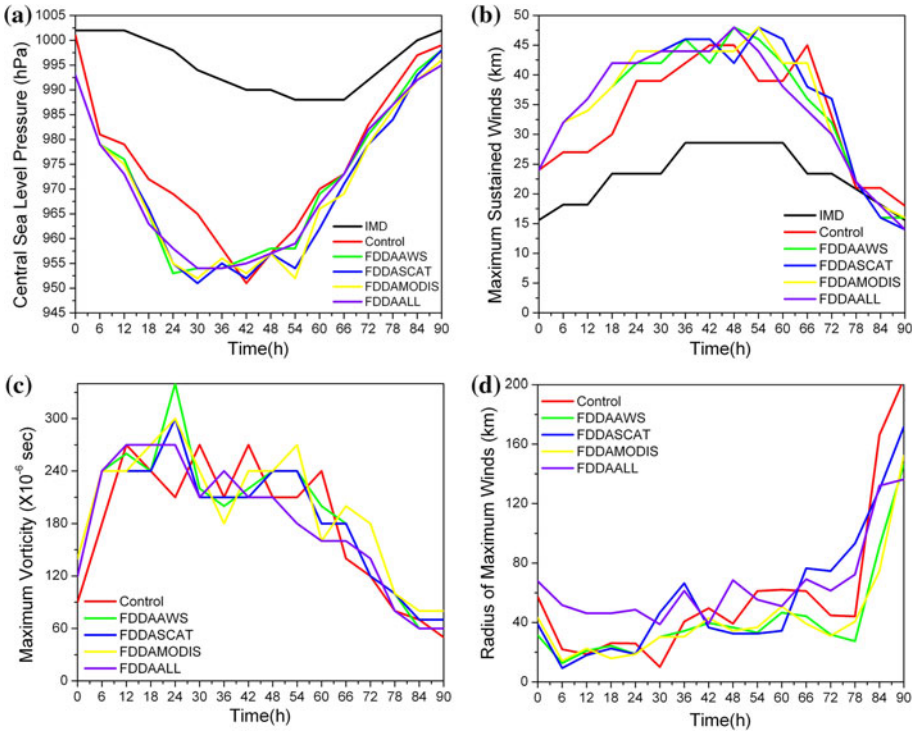

Fig. 7 Time evolution of **a** MSLP, **b** MSW, **c** Vorticity and **d** radius of maximum winds from different real-time prediction experiments

different observations are started at 18 UTC 03 Nov, and the first 12 h of simulation is treated as pre-forecast period and the actual forecast begins from 06 UTC 04 Nov. The control run is started at 06 UTC 04 Nov. The difference in these experiments is related to the data given for model initialization and boundary condition. The results from these four experiments in respect of CSLP, MSW, vorticity, radius of maximum winds and geopotential are discussed below, with comparisons using IMD estimates wherever possible.

5.2.1 Intensity of the simulated storm

The time evolution of the CSLP from the control (CTL) and different assimilation experiments is shown in Fig. 7a from 06 UTC Nov 4 to 00 UTC Nov 9. The CTL run indicates a pre-deepening period of 6 h up to 18 UTC 04 Nov, and then a steep deepening period of 24 h up to 00 UTC 06 Nov. Thereafter, the storm in the CTL run has shown gradual weakening. All the three assimilation experiments have a pre-deepening period of 6 h up to 18 UTC 04 Nov and a deepening period of 21 h up to 09 UTC 05 Nov. The lowest CSLP in the control and assimilation experiments was about 950 hPa, which indicates a maximum central pressure drop of 50 hPa, attained after 27 h of simulation in the assimilation experiments and 42 h in the control run. While both the FDDAMODIS and the FDDASCAT give the same time variation of CSLP throughout the simulation, the FDDAAWS has given slightly higher CSLP (relatively higher pressure drop) after 36 h of simulation, that is, after 12 UTC 06 Nov indicating a less intense storm than that in the

other two FDDA runs. As noted earlier, the IMD estimates indicate the maximum winds to increase rapidly from 30 to 66 h (between 12 UTC 06 Nov to 00 UTC 07 Nov). The time variation of maximum winds (Fig. 7b) indicates both the Control and the FDDA runs produced the above trend of intensification and weakening of the storm but 12 h earlier than the actual intensification and weakening. While the control run produced the lowest maximum winds of all the four experiments, the FDDASCAT and FDDAALL produced the highest MSW but with a drop in intensity between 42 and 60 h (between 00 UTC 06 Nov to 18 UTC 06 Nov) followed by FDDASCAT, FDDAMODIS and FDDAAWS. The time variation of maximum vorticity of the storm at 925 hPa from CTL and the three FDDA experiments is given in Fig 7c. The highest vorticity in the CTL run is about 275×10^{-5} s^{-1}, which seems to occur at 00 UTC 07 Nov, while that in FDDASCAT (300×10^{-5} s^{-1}) occurred at 18 UTC 05 Nov, that is, in very early stages of storm development. But this experiment also gives a second maximum in vorticity of 240×10^{-5} s^{-1} at 00 UTC 07 Nov after 72 h of simulation. The maximum vorticity evolution in both FDDAWS and FDDAMODIS is nearly similar, and the highest vorticity in these two experiments is about 300×10^{-5} s^{-1}, which occurred after 54 h of simulation, that is, at 18 UTC 05 Nov. The vorticity evolution of FDDAMODIS is more realistic as it produced the highest value during the mature stage of the storm. The time evolution of the radius of maximum winds from the CTL and the three FDDA simulations is presented in Fig. 7d. On an average, the RMW varied as 50 to 80 km in the deepening and mature stage of the storm and as 100 km in the dissipating stage. It is seen that while FDDAAWS and FDDAMODIS produce the lowest RMW ($\sim$40 km), the FDDASCAT and FDDAALL produced the highest RMW ($\sim$80 km) with CTL run giving intermediate values. All the experiments show the highest RMW after 78 h of simulation, that is, after 12 UTC 07 Nov. The lowest RMW is given by FDDAMODIS at 66 h of simulation during the highest intensification stage thus giving a more realistic simulation.

The sea level pressure distribution is plotted from CTL and various FDDA experiments and is shown in Fig. 8 along with the IMD surface synoptic chart corresponding to the time at 00 UTC 07 Nov when the storm attained its highest intensification. The IMD chart shows a positive gradient of sea level pressure from a peripheral value of 1,010 hPa at equator and a major portion of southern Peninsular India and decreasing to the centre of the cyclone with a central value of 996 hPa. The sea level pressure was about 1,012 hPa over the central India, Indian Ocean near to Mynmar and Andaman Islands. The pressure distribution from simulations, although agrees in the peripheral region covering up to SriLanka and south Tamil Nadu, a higher drop relative to IMD values in central pressure is simulated in all the experiments indicating stronger simulated cyclones. The central pressures are simulated as 960 hPa in CTL run, 957 hPa in FDDAAWS as well as in FDDAALL, 954 hPa in FDDASCAT and 953 hPa in FDDAMODIS. Thus, the simulations FDDAMODIS and FDDASCAT both give a more intensive cyclone than the FDDAAWS and CTL runs.

The spatial distribution of vorticity pattern from CTL and FDDA experiments at 00 UTC 07 Nov along with the CIMSS Meteosat vorticity image is presented in Fig. 9. The CIMSS vorticity image shows the highest positive vorticity to be distributed about 12.50° N, 83.0° E, with the location of the storm at 13.0° N, 83.0° E. The observed vorticity is in the range of 100×10^{-5} to 250×10^{-5} s^{-1}. Comparison of model vorticity with CIMSS image indicates that the cyclonic vorticity in the CTL run is predicted to the south of the observed vorticity distribution and that the centre of positive vorticity in all FDDA runs matches with the observed maximum vorticity distribution. This indicates that the location of cyclone at its highest intensification stage could be simulated better in the FDDA

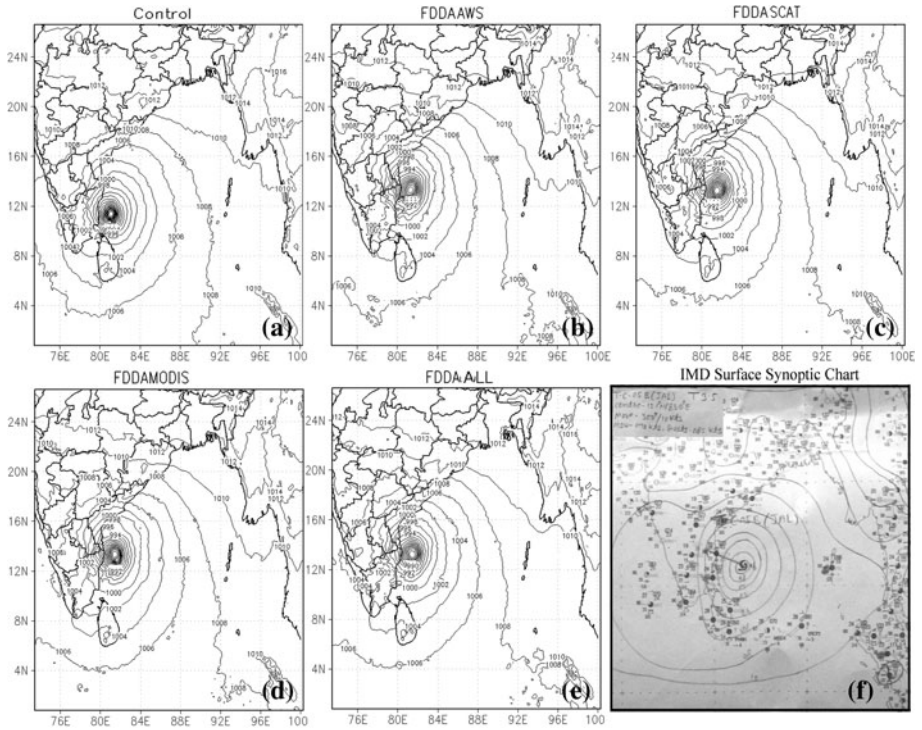

Fig. 8 Comparison of sea level pressure at 00 UTC 07 Nov from **a** CTL, **b** FDDAAWS, **c** FDDASCAT, **d** FDDAMODIS and **e** FDDAALL and **f** IMD surface synoptic chart

experiments than in the control run. The simulations reveal a positive vorticity pattern around the cyclone in the range 0–200 $\times$ 10^{-5} s^{-1} and a negative vorticity pattern of up to 20 $\times$ 10^{-5} s^{-1} in the region outside the cyclone. Of all these assimilation runs, the FDDAMODIS indicates vorticity bands of 50 $\times$ 10^{-5} to 250 $\times$ 10^{-5} s^{-1}, with both location and distribution agreeing with the CIMSS vorticity image. Thus, considering all the parameters (CSLP, MSW, Vorticity, RMW and Geopotential), the experiments FDDASCAT and FDDAMODIS seem to give the highest intensive cyclone closely agreeing with the IMD estimates of intensity of the storm.

5.2.2 Movement of the simulated storm

The movement of the simulated storm is analysed by comparing the computed track positions with the IMD best-track estimates (Fig. 10). It is seen that in the CTL run, the storm moves to the south of the observed storm after 12 h of simulation and makes a landfall about 50 km south of Chennai city. In all the experiments, the simulated storm is noted to move faster than the actual storm thereby producing along track errors. The simulated storm in all the FDDA runs has moved north of the observed storm, and the track positions were almost similar. The landfall point of the simulated storm in the FDDA runs is within 25–75 km north of Chennai city, the nearest track is from FDDAMODIS and FDDASCAT, which simulated the landfall of the cyclone about 50 km north of Chennai city. The initial track position errors are noted to vary as 89–58 km in control and different

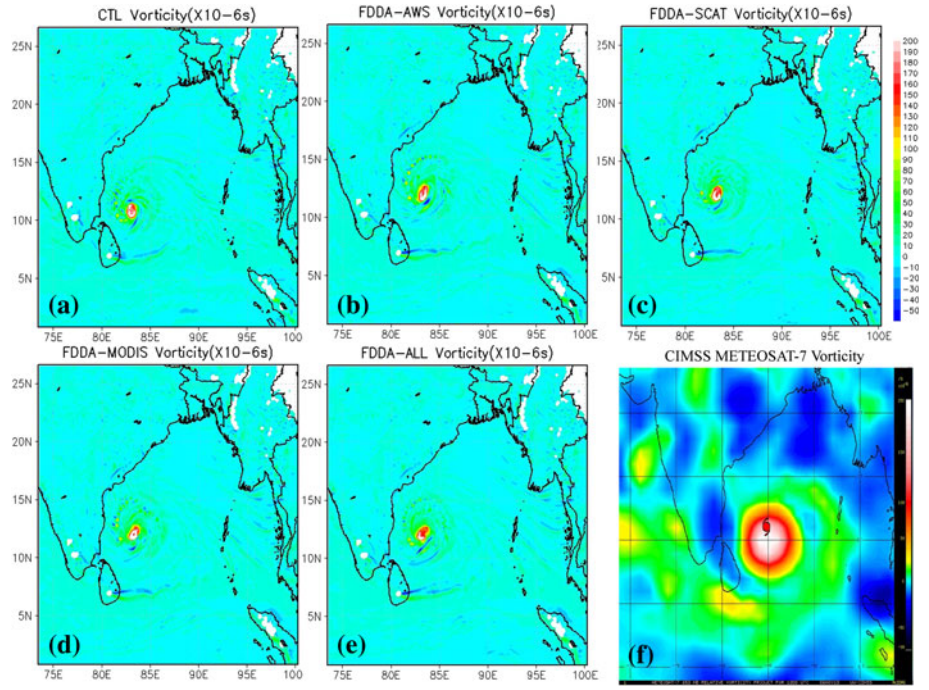

Fig. 9 Model simulated vorticity (×10e−5) at 850 mb at 12 UTC 06 Nov from **a** CTL run, **b** FDDAAWS, **c** FDDASCAT, **d** FDAMODIS, **e** FDDAALL and **f** CIMSS MeteosatVorticity image

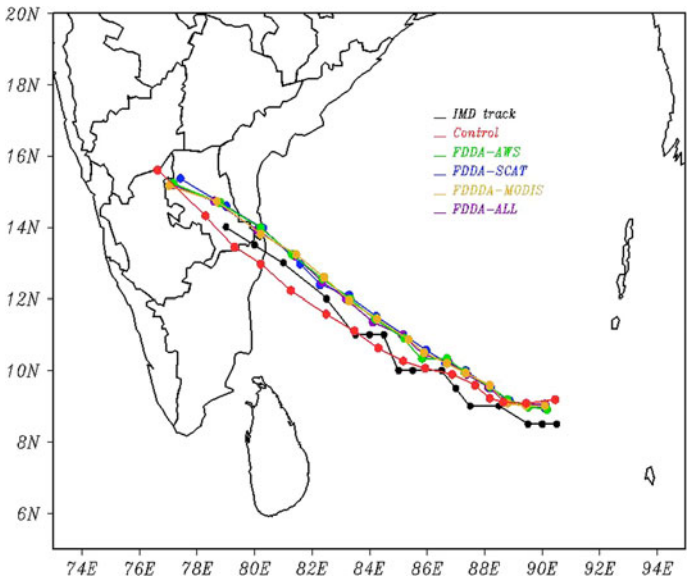

Fig. 10 Track positions of the simulated storm from assimilation experiments

Table 5 Vector track errors in control and various assimilation experiments

Simulation	Vector track errors in km								
	Hours of simulation								
	0	12	24	36	48	60	72	84	90
Control Run	89.4	43.3	45.6	46.8	115.2	283.3	194.4	317.7	397.7
FDDAAWS	58.9	109.3	108.4	83.8	183.6	252.4	335.9	399.9	410.2
FDDASCAT	66.9	100.9	111.4	86.3	225.9	144.1	147.6	207.0	295.7
FDDAMODIS	72.7	101.8	104.1	87.2	179.9	249.2	324.0	388.0	376.0
FDDAALL	69.7	107.4	93.2	91.5	189.2	243.7	333.0	387.8	321.1

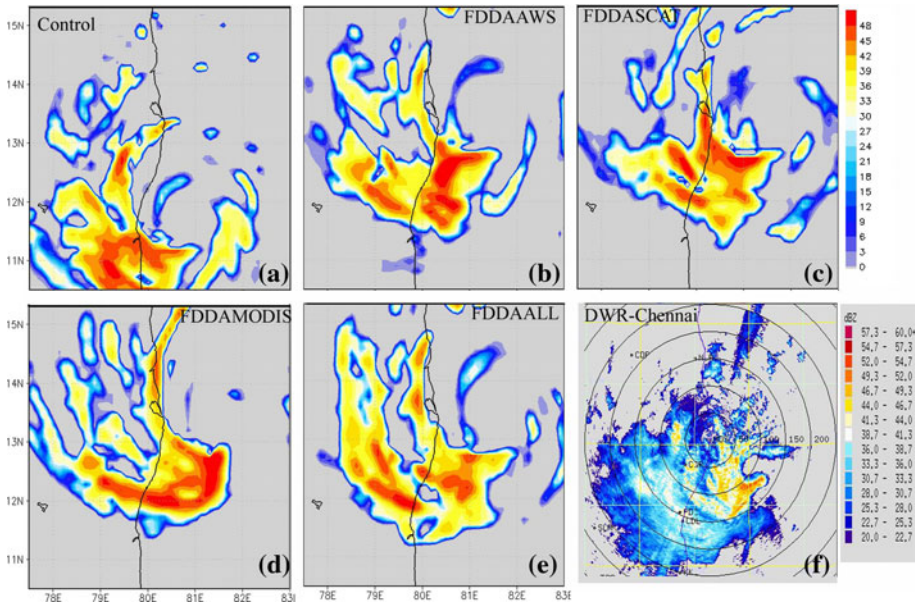

Fig. 11 Simulated radar reflectivity from **a** CTL run, **b** FDDAAWS, **c** FDDASCAT, **d** FDDAMODIS, **e** FDDAALL and **f** DWR observed reflectivity corresponding to 03 UTC 07 Nov

assimilation experiments (Table 5). In the control run, the track errors are of the order of 89 km in the first 12 h, 45 km after 12 h, 115 km at, 48 h, 194 km at 72 h and >300 km after 72 h of simulation, respectively (Table 5). The track errors in the FDDA runs are below 70 km in the first 24 h, increased to 175 km in 48 h, and thereafter further increased to 325 km except FDDASCAT. The FDDASCAT produced least track errors in the deepening and dissipation phase with overall errors ranging from 66 to 250 km. Next to FDDASCAT, FDDAMODIS produced lesser errors.

5.2.3 Simulated spatial cloud band structure

Simulated cloud band structure of JAL cyclone from different simulations is analysed at the landfall time corresponding to 03 UTC 07 Nov using simulated radar reflectivity and

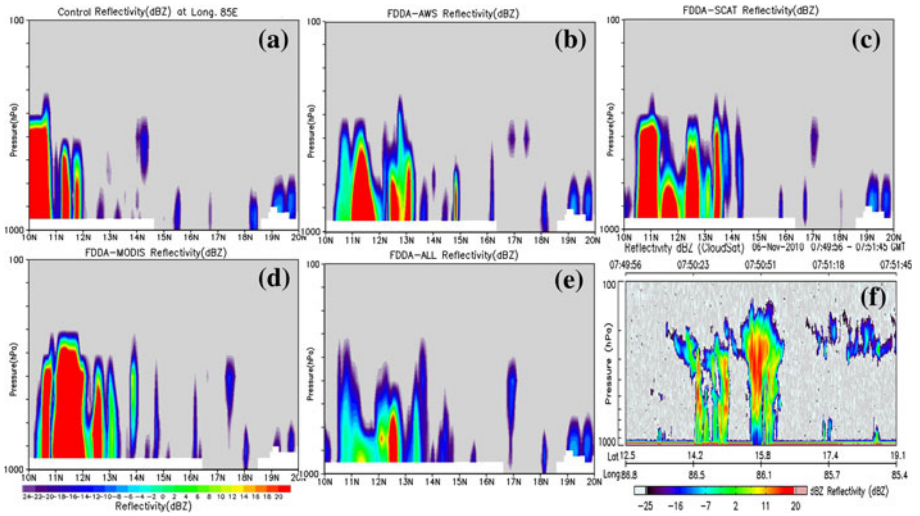

Fig. 12 Vertical section of simulated reflectivity from **a** CTL run, **b** FDDAAWS, **c** FDDASCAT, **d** FDDAMODIS, **e** FDDAALL and **f** CloudSat observed reflectivity at 0750 UTC 06 Nov at 85 E

compared with DWR radar reflectivity (Fig. 11). It is well known that in mature tropical cyclones, the clouds organize in spiral bands around the central calm area called the 'eye' region. All the simulations show a comma cloud organization around the cyclone. The dense cloud bands are noted to be distributed in the southwest sector in Control run, southern sector in the FDDAAWS, south-southeast in FDDASCAT, southeast sector in FDDAMODIS and in roughly circular symmetry in FDDAALL, respectively, indicating the location of maximum distribution in the respective simulations. The reflectivity pattern obtained from FDDASCAT and FDDAMODIS is noted to closely compare with the DWR reflectivity (Fig. 11f). The FDDASCAT gives a denser spiral band cloud region around the eye in the southeast sector with less outward extension of clouds, whereas the FDDAMODIS produces dense cloud bands in the southern sector as well as the outward extension of clouds.

The vertical organization of convective clouds around the cyclone is analysed from the cross-section of simulated radar reflectivity in north–south plane at 85° E from different simulations, and their comparison with CloudSat observed reflectivity corresponding to 0750 UTC 06 Nov due to the availability of observations at this time (Fig. 12). Observed reflectivity data show the wall cloud region distributed around the central calm region. The clouds are densely distributed on the northern sector with deep cores of convective organization reaching almost up to 200 hPa. In the simulations, the wall cloud region is distributed in 11 N–13 N in the control run, 10.5 N–15 N in FDDAAWS, MODIS, 11 N–15 N in FDDASCAT, 10.5 N–13.5 Nin FDDAALL and with vertical extent up to 400 hPa. Of all the simulations, the FDDASCAT and FDDAMODIS are seen to produce nearest reflectivity pattern.

5.2.4 Simulated rainfall

The simulated rainfall pattern from CTL and various FDDA experiments during the landfall time is compared with TRMM rainfall pattern. The simulated accumulated rainfall

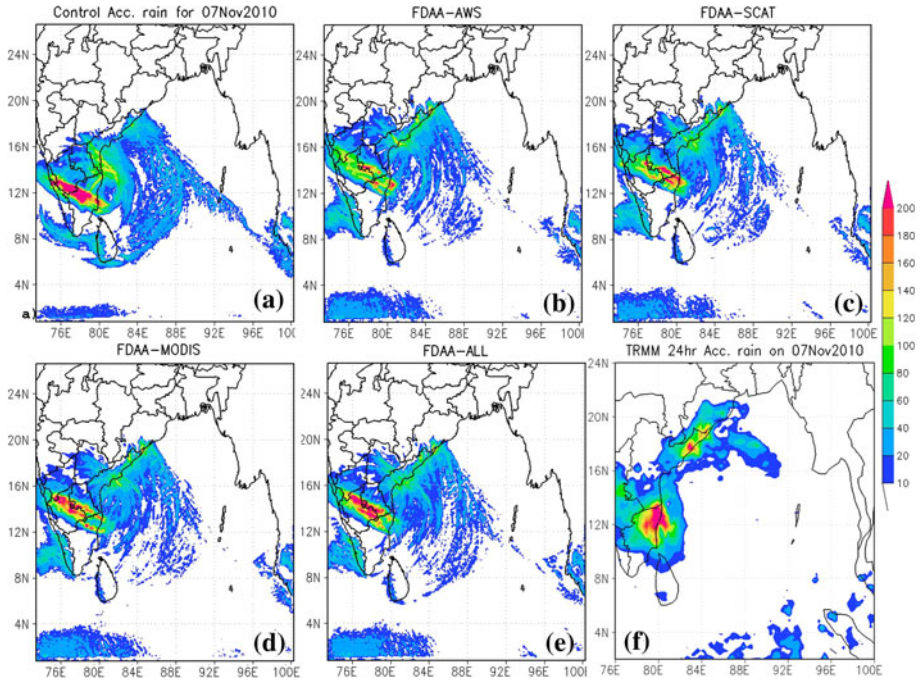

Fig. 13 Model simulated 24 h accumulated rainfall in different experiments for the period ending at 00 UTC 8 Nov **a** CTL run, **b** FDDAAWS, **c** FDDASCAT, **d** FDDAMODIS **e** FDDAALL and **f** TRMM rainfall

for the 24-h period from 00 UTC 07 Nov to 00 UTC 08 Nov along with the corresponding TRMM observed rainfall is plotted in Fig. 13. As mentioned in the previous section in 2.1.3, the TRMM data for experiment 00 UTC 08 Nov indicate concentration of maximum rainfall ($\geq$200 mm) along the north Tamil Nadu coast and the adjoining land, ocean regions with gradually southward decreasing rainfall. Rainfall bands in the range 120–10 mm are noted to spread in the entire southern peninsular India barring parts of extreme south Tamil Nadu and south Kerala. A second spatial peak of rainfall is seen along the north coastal Andhra Pradesh around Visakhapatnam. The CTL and FDDA experiments show the rainfall distribution, indicating maximum rainfall in the central eye wall region according to the simulated storm location, but none have produced the observed rainfall pattern. In the experiments CTL and FDDAMODIS, the central rainband appears to have shifted about 350 km inland from the observed peak rainfall pattern and to have an elongation in northwest–southeast directions. This shows that the model storm had moved faster than the actual one in the above experiments. In the experiments FDDAAWS and FDDASCAT, the location of the central rain band was slightly shifted to about 50–75 km inland in the northwest direction and with an elongation in the northwest and southeast directions. The precipitation in these two experiments has spread to the northern Tamil Nadu and south Andhra Pradesh. The rainfall simulated in FDDASCAT appears to be more closer to the TRMM rainfall pattern, which shows the observed higher rainfall amounts of 100–200 mm in the northern Tamil Nadu and adjoining coastal parts.

6 Summary and conclusion

Prediction of the movement and intensification of tropical cyclones is very important for cyclone disaster management in the coastal regions and is a challenging problem. Numerical models with appropriate initial conditions need to be developed to provide precise forecasts. The present work examines the performance of a mesoscale model driven by different initial conditions derived from GFS analysis and forecasts corresponding to its various analysis cycles and the impact of nudging of various observations (conventional, satellite based) on the simulated cyclone characteristics. For this purpose, a double-nested non-hydrostatic model WRF ARW is employed. The recent severe tropical cyclone in the Bay of Bengal near Tamil Nadu during 4 to 8 November 2010 is studied. Real-time ARW mesoscale model predictions are made with 11 different initial conditions between 00 UTC 04 Nov to 12 UTC 06 Nov using six hourly GFS analysis and forecasts. Results from these eleven experiments indicated that simulations starting prior to 18 UTC 04 Nov produced relatively higher intensification in terms of drop in central sea level pressure with relatively longer pre-deepening period. The peak intensification in different prediction experiments occurred successively at 6 h later relative to the experiment 00 UTC 04 Nov. The CSLP pattern from the experiments 18 UTC 04 Nov and 00 UTC 05 Nov agreed with the IMD reports, which indicated the storm had attained peak intensity of severe cyclone between 18 UTC 06 Nov and 00 UTC 07 Nov and gradually weakened thereafter.

The series of real-time simulations showed a progressive decrease in the intensity from experiments starting at early phase to those in depression phase. The time series of maximum winds as well as central pressure indicated an early intensification and early weakening than the actual cyclone for the experiments starting prior to 18 UTC 04 Nov. The experiments 18 UTC 04 Nov, 00 UTC 05 Nov, 06 UTC 05 Nov produced a more realistic time evolution of MSW very closely following the IMD estimates. The experiments starting subsequent to 06 UTC 05 Nov all produced successively far lesser intensification compared to those starting earlier to 06 UTC 05 Nov with the experiment 12 UTC 06 Nov, producing the lowest intensity of all with predicted MSW of 35 m/s. These results demonstrate that experiments starting at different times during the life cycle of the cyclone produce different results, that is, experiments with initial condition during low pressure stage produced an early intensification as well as early decay with an overall higher intensification in comparison with the observed characteristics. On the other hand, experiments starting in the mature stage/severe cyclone stage (i.e., after 12 UTC 06 Nov) have produced a late intensification of the storm with relatively less intensification. The errors in the late phase experiments may be due to less spin-up time for the model to evolve the cyclone. Simulations beginning from the low pressure to depression phase produced more realistic simulation of the life cycle in terms of intensification/decay characteristics than the rest. The above results suggest that a minimum simulation period of 48 h with initial conditions defined at the pre-deepening/deepening phase may be necessary to evolve a proper life cycle of the storm. The experiment 18 UTC 04 Nov produced a gradually growing vorticity during intensification and a decaying vorticity during weakening phase, thus produced a more realistic time variation of vorticity associated with the cyclone. The experiment starting at 18 UTC 04 Nov produced the lowest RMW of about 50 km during the peak intensification stage and also more realistic values of RMW ($\sim$75 km) during the weakening phase.

The track positions from various real-time experiments indicate northwestward moving cyclone with divergent tracks after 00 UTC 05 Nov. The predicted cyclone tracks are aligned to the south of the observed track in the experiments starting prior to 18 UTC 04

Nov and to the north of the IMD estimated track in the experiments starting after 18 UTC 04 Nov with successive northward incremental drifts in the track positions. The vector track errors gradually increased from initial time in various experiments with largest errors up to $\sim$250 km noted with experiments 00 UTC 04 Nov, 12 UTC 04 Nov, 06 UTC 12 Nov and 12 UTC 05 Nov, respectively. The experiment 18 UTC 04 Nov has given marginal errors right from the beginning of the simulations agreeing closely with the IMD estimated track. Considering both the intensity and the movement, the simulation 18 UTC 04 Nov produced the best prediction.

To examine the impact of assimilation of available observations on the predictions, FDDA analysis nudging was performed separately for 12-h pre-forecast period prior to 06 UTC 04 Nov with land-based conventional surface observations (FDDAAWS), satellite-based winds (ASCAT, OCEANSAT) (FDDASCAT) and MODIS surface temperature (FDDAMODIS). These experiments reduced the pre-deepening period of the storm by nearly 12 h. While both FDDASCAT and FDDAMODIS produced similar CSLP drop as in control run, the assimilation of AWS data has given a marginal improvement in the intensity of storm. The FDDASCAT produced higher MSW and an unrealistic drop in intensity between 00 UTC 05 Nov to 12 UTC 06 Nov. The vorticity evolution of FDDAMODIS is found more realistic with relatively highest values (275×10^{-5} s^{-1}) during the mature stage of the storm after 18 UTC 06 Nov. It also produced vorticity bands of 50×10^{-5} to 250×10^{-5} s^{-1} in well agreement with the CIMSS vorticity distribution in location and distribution. The time evolution of radius of maximum winds from control and assimilation experiments indicated that the lowest RMW of 35 km is given by FDDAMODIS at 00 UTC 07 Nov during the highest intensification stage thus giving a more realistic simulation. Comparisons with surface synoptic charts indicate, though, the pressure distribution is well simulated in the peripheral region, relatively stronger cyclones are simulated in all cases with FDDAMODIS and FDDASCAT giving a more intensive cyclone than the FDDAAWS and CTL runs. Thus, considering all the parameters (CSLP, MSW, Vorticity, RMW and Geopotential), the experiments FDDASCAT and FDDAMODIS have given highest intensive cyclone with trends matching with the IMD estimates of intensity of the storm. A significant improvement is noted in the simulated track positions in the assimilation experiment FDDAMODIS over the control run. The control run produced track moved to the south of IMD estimated track after 12 h of simulation and produced an error of about 100 km, while that from the FDDAMODIS, though, has errors initially approached the IMD estimated track after 18 h of simulation, giving a landfall point about 50 km to the north of estimated track. As the simulated cyclone in all the experiments moved faster than the actual storm, the simulated rainfall appears to have shifted about 100–250 km inland from the observed peak rainfall pattern and to have an elongation in northwest-southeast directions. The rainfall simulated in FDDASCAT appears to be more closer to the TRMM rainfall giving a distribution of 100–200 mm in the northern Tamil Nadu and adjoining coastal parts.

Acknowledgments Authors sincerely thank Sri S. C. Chetal, Director, IGCAR, Dr. R. Baskaran, for their encouragement in carrying out the study. The NCEP GFS analysis and forecasts were obtained from NCEP. The ASCAT data were obtained from EUMETSAT. Thanks are due to Dr. B. Manikiam and Dr. Kusuma Rao, ISRO, for providing AWS observations as part of PRWONAM mesoscale program from MOSDAC, SAC, Ahmadabad. The India Meteorological Department is acknowledged for the use of best-track and intensity estimates, Synoptic charts, AWS Data and the DWR reflectivity composites of tropical cyclones. Cloud-sat reflectivity composites are obtained from NASA GES DISC. The MODIS data were downloaded from NOAA. The authors acknowledge ISRO for providing OCEANSAT vector wind data for the study.

References

Bhaskar Rao DV, Hari Prasad D (2006) Numerical prediction of the Orissa super-cyclone (2006): sensitivity to the parameterization of convection, boundary layer and explicit moisture processes. Mausam 57(1):61–78

Bhaskar Rao DV, Hari Prasad D (2007) Sensitivity of tropical cyclone intensification to boundary layer and convective processes. Nat Hazards 41(3):429–445

Bhaskar Rao DV, Hari Prasad D, Srinivas D (2009a) Impact of horizontal resolution and the advantages of the nested domains approach in the prediction of tropical cyclone intensification and movement. J Geophys Res 114:D11106. doi:10.1029/2008JD011623

Bhaskar Rao DV, Srinivas D, Hari Prasad D (2009b) Real time prediction of SIDR cyclone over Bay of Bengal using high resolution mesoscale models. In: Charabi Y (ed) Indian Ocean tropical cyclones and climate change. Springer, Berlin

Bi L, NRL Monterey CA, Jung J, Santek DA, Morgan MC (2010) Quantification of forecast impact of ASCAT surface winds assimilated into NCEP's GFS model. In: 14th Symposium on integrated observing and assimilation systems for the atmosphere, oceans, and land surface (IOAS-AOLS). American Meteorological Society, Atlanta, GA

Chen DR, Yeh TC, Haung KN, Peng MS, Chang SW (1995) A new operational typhoon track prediction system at the central weather Bureau in Taiwan. In: 21st conference hurricane tropical meteorological society, Boston, MA (preprints)

Davis C, Wang W, Chen SS, Chen Y, Kristen C, Mark D, Dudhia J, Holland G, Klemp J, Michalakes J, Reeves H, Rotunno R, Snyder C, Xiao Q (2008) Prediction of landfalling hurricanes with the advanced hurricane WRF Model. Mon Wea Rev 136:1990–2005

Deshpande M, Pattnaik S, Salvekar PS (2010) Impact of physical parameterization schemes on numerical simulation of super cyclone Gonu. Nat Hazards 55:211–231

Dudhia J (1989) Numerical study of convection observed during winter monsoon experiment using a mesoscale two-dimensional model. J Atmos Sci 46:3077–3107

Gray WM (1968) Global view of the origin of tropical disturbances and storms. Mon Wea Rev 96:669–700

Hong SY, Noh Y, Dudhia J (2006) A new vertical diffusion package with explicit treatment of entrainment processes. Mon Wea Rev 134:2318–2341

IMD (2011). Report on cyclonic disturbances over North Indian Ocean during 2010. RSMC-Tropical Cyclone Report no. 1/2011. India Meteorological Department. Jan. 2011

Iwasaki T, Nakano H, Sugi M (1987) The performance of typhoon track prediction model with cumulus parameterization. J Meteorol Soc Jpn 65:555–570

Kain JS (2004) The Kain-Fritsch convective parameterization: an update. J Appl Meteorol 43:170–181

Kain JS, Fritsch JM (1993) Convective parameterization for mesoscale models: The Kain-Fritcsh scheme. In: Emanuel KA, Raymond DJ (eds) The representation of cumulus convection in numerical models. American Meteorological Society, 246 pp

Kalnay E (2003) Atmospheric modeling, data assimilation and predictability. Cambridge University Press, Cambridge

Kim YH, Jeon EH, Chang DE, Lee HS, Park JI (2010) The impact of TPARC 2008 dropsonde observations on typhoon track forecasting. Asia-Pacific J Atmos Sci 46:287–303

Kurihara Y, Bender MA, Tuleya RE, Ross RJ (1993) Hurricane forecasting with GFDL hurricane prediction system. In: 21st Conference hurricane tropical meteorological society, Boston, MA, pp 323–326 (preprints)

Langland RH, Velden C, Panley PM, Berger H (2009) Impact of satellite-derived rapid-scan wind observations on numerical model forecasts of hurricane Katrina. Mon Wea Rev 137:1615–1622

Leslie LM, LeMarshall JF, Morison RP, Spinoso C, Purser RJ, Pescod N, Seecamp R (1998) Improved hurricane track forecasting from the continuous assimilation of high quality satellite wind data. Month Wea Rev 126:1248–1257

Lin YL, Farley RD, Orville HD (1983) Bulk parameterization of the snow field in a cloud model. J Climate Appl Meteorol 22:1065–1092

Marshall JL, Leslie L, Morrison R, Pescod N, Seecamp R, Spinoso C (2000) Recent developments in the continuous assimilation of satellite wind data for Tropical cyclone forecasting. Adv Space Res 25(25):1077–1080

Mathur MB (1991) The national Meteorological Center's quasi-Lagrangian model for hurricane prediction. Mon Wea Rev 109:1419–1447

Mlawer EJ, Taubman SJ, Brown PD, Iacono MJ, Clough SA (1997) Radiative transfer for inhomogeneous atmosphere: RRTM, a validated correlated-k model for the longwave. J Geophys Res 102(D14): 16663–16682

Mohanty UC, Mandal M, Raman S (2004) Simulation of Orissa super-cyclone (1999) using PSU/NCAR mesoscale model. Nat Hazards 31:373–390

Mukhopadhyay P, Sanjay J, Cotton WR, Singh SS (2004) Impact of surface meteorological observation on RAMS forecast of monsoon weather systems over the Indian region. Meteorol Atmos Phys 90:77–108

Navon IM (2009) Data assimilation for numerical weather prediction: a review. In: Park SK, Xu L (eds) Data assimilation for atmospheric, oceanic and hydrologic applications. Springer, Berlin, pp 21–65

OSI SAF (2010) ASCAT wind product user manual version 1.8. Ocean and Sea Ice SAF. SAF/OSI/CDOP/KNMI/TEC/MA/126

Park SK, Zhang DL, Kim HH (2008) Impact of dropwindsonde data on the track forecasts of a tropical cyclone: an observing-systems simulation experiment study. Asia-Pacific J Atmos Sci 44:85–92

Pattnayak S, Mohanty UC (2008) A comparative study on performance of MM5 and WRF models in simulation of tropical cyclones over Indian seas. Curr Sci 95:923–936

Pattnayak DR, Rama Rao YV (2009) Track prediction of very severe cyclone 'Nargis' using high resolution weather research forecasting (WRF) model. J Earth Syst Sci 118(4):309–329

Prasad K, Rama Rao YV (2003) Cyclone track prediction by a quasi-Lagrangian limited area model. Meteorol Atmos Phys 83:173–185

Pu Z (2009) Assimilation of satellite data in improving numerical simulation of tropical cyclones: progress, challenge and development. In: Park SK, Xu L (eds) Data assimilation for atmospheric, oceanic and hydrologic applications. Springer, Berlin, pp 163–176

Puri K, Davidson NE, Leslie LM, Lagan LW (1992) The BMRC tropical limited area model. Aust Meteorol Mag 40:81–104

Raghavan S, Sen Sarma AK (2000) Tropical cyclone impacts in India and neighbourhood. In: Pielke R Jr, Pielke R Sr (eds) Storms, vol 1. Routledge, London, pp 339–356

Rao KG (2008) PRWONAM for Mesoscale Monsoon Research in India and predictions over SHAR-Kalpakkam—Bangalore Region. Technology Development for Atmospheric Research & Applications, pp 193–230

Roy Bhowmik SK (2003) Prediction of monsoon rainfall with a nested grid mesoscale limited area model. Proc Indian Acad Sci Earth Planet Sci 112:499–519

Sandeep S, Chandrasekar A, Singh D (2006) The impact of assimilation of AMSU data for the prediction of a tropical cyclone over India using a mesoscale model. Int J Remote Sens 27:4621–4653

Singh R, Pal PK, Kishtawal CM, Joshi PC (2008) The impact of variational assimilation of SSM/I and QSCAT satellite observations on the numerical simulation of Indian Ocean Tropical Cyclones. Wea Forecast 23:460–476

Skamarock WC, Klemp JB, Dudhia J, Gill DO, Barker DM, Dudha J, Huang X, Wang W, Powers Y (2008) A description of the advanced research WRF Ver.30. NCAR technical note. NCAR/TN-475 + STR. Mesocale and Microscale Meteorology Davison, National Centre for Atmospheric Research, Boulder Colorado, USA, p 113

Soden BJ, Velden CS, Tuleya RE (2001) The impact of satellite winds on experimental GFDL hurricane model forecasts. Mon Wea Rev 129:835–852

Srinivas CV, Venkatesan R, Bhaskar Rao DV, Hariprasad D (2007) Numerical simulation of andhra severe cyclone (2003): model sensitivity to boundary layer and convection parameterization. Pure Appl Geophys 164:1–23

Srinivas CV, Venkatesan R, Vesubabu V, Nagaraju C (2010a) Impact of assimilation of conventional and satellite meteorological observations on the numerical simulation of a Bay of Bengal Tropical Cyclone of Nov 2008 near Tamilnadu using WRF model. Meteorol Atmos Phys 110:19–44. doi:10.1007/s00703-010-0102-z

Srinivas CV, Yesubabu V, Nagaraju C, Venkatesan R, Chellapandi P, Raj B (2010b) Assimilation of conventional and satellite wind observations in a mesoscale atmospheric model for studying atmospheric dispersion. Atmos Environ 44:2846–2864

Stauffer DR, Seaman N (1990) Use of four-dimensional data assimilation in a limited-area mesoscale model. Part I: experiments with synoptic-scale data. Mon Wea Rev 118:1252–1277

Stauffer DR, Seaman NL (1994) Multiscale four-dimensional data assimilation. J Appl Meteorol 33:416–434

Stauffer DR, Seaman N, Binkowski FS (1991) Use of four-dimensional data assimilation in a limited-area mesoscale model. Part II: effects of data assimilation within the planetary boundary layer. Mon Wea Rev 119:734–754

Takahashi M (2010) Operational use of scatterometer winds in the JMA data assimilation system. International Ocean Vector Winds Science Team Meeting, JMA, Barcelona, Spain, 18–20 May 2010

Vinodkumar V, Chandrasekhar A, Alapaty K, Niyogi DS (2007) The effect of a surface data assimilation technique and the traditional four-dimensional data assimilation on the simulation of a monsoon depression over India using a mesoscale model. Nat Hazards 42:439–453

Wu CC, Chou KH, Lin PH, Aberson SD, Peng MS, Nakazawa T (2007) The impact of dropwindsonde data on typhoon track forecast in DOTSTAR. Wea Forecast 22:1157–1176

Zhang X, Xiao Q, Fitzpatrick PJ (2007) The impact of multisatellite data on the initialization and simulation of Hurricane Lili's (2002) rapid weakening phase. Adv Atmos Sci 22(4):534–544

Zhihua Z, Yihong D, Xudong L, Leiming M, Chan JC (2005) The effect of three-dimensional variational data assimilation of QSCAT data on the numerical simulation of typhoon track and intensity. Adv Atmos Sci 22(4):534–544